August 1992

Control of Rolling Contacts in Multi-Arm Manipulation

Eric Paljug
University of Pennsylvania

Xiaoping Yun
University of Pennsylvania

R. Vijay Kumar
University of Pennsylvania, kumar@grasp.upenn.edu

Control of Rolling Contacts in Multi-Arm Manipulation

Abstract

When multiple arms are used to manipulate a large object, it is beneficial and sometimes necessary to maintain and control contacts between the object and the effector (the contacting surface of an arm) through force closure. Rolling and/or sliding can occur at these contacts, and the system is characterized by holonomic as well as nonholonomic (including unilateral) constraints. In this paper, the control of planar rolling contacts is investigated. Multi-arm manipulation systems are typically redundant. In our approach, a minimal set of inputs is employed to control the trajectory of the system while the surplus inputs control the contact condition. The trajectory includes the gross motion of the object as well as the rolling motion at the contacts. A nonlinear feedback scheme for simultaneous control of motion as well as contact conditions is presented. A new algorithm which adapts a two-effector grasp with rolling contacts to external loads and the trajectory is developed. Simulations and experimental results are used to illustrate the salient features in control and planning.

Comments

Control of Rolling Contacts In Multi-Arm Manipulation

MS-CIS-92-65
GRASP LAB 329

Eric Paljug
Xiaoping Yun
Vijay Kumar

August 1992

Control of Rolling Contacts in Multi-Arm Manipulation

Eric Paljug, Xiaoping Yun, and Vijay Kumar

General Robotics and Active Sensory Perception (GRASP) Laboratory
University of Pennsylvania
3401 Walnut Street, Room 301C
Philadelphia, PA 19104-6228

ABSTRACT

When multiple arms are used to manipulate a large object, it is beneficial and sometimes necessary to maintain and control contacts between the object and the effector (the contacting surface of an arm) through force closure. Rolling and/or sliding can occur at these contacts, and the system is characterized by holonomic as well as nonholonomic (including unilateral) constraints. In this paper, the control of planar rolling contacts is investigated. Multi-arm manipulation systems are typically redundant. In our approach, a minimal set of inputs is employed to control the trajectory of the system while the surplus inputs control the contact condition. The trajectory includes the gross motion of the object as well as the rolling motion at the contacts. A nonlinear feedback scheme for simultaneous control of motion as well as contact conditions is presented. A new algorithm which adapts a two-effector grasp with rolling contacts to external loads and the trajectory is developed. Simulations and experimental results are used to illustrate the salient features in control and planning.

1 Introduction

There are numerous examples of manipulation tasks involving large (possibly, but not necessarily heavy), awkwardly sized payloads such as cartons, crates and barrels that cannot be grasped by one end-effector or hand. Instead of designing large end-effectors, which then require large robots (which becomes impractical beyond a point), the logical solution is to employ multiple, relatively small robots, in order to enhance the grasping capability. Further, it is attractive to allow palms, forearms and other surfaces of robot limbs to contact the object as opposed to fingertip grasping or dual arm manipulation with two end-effectors, in which contacts are restricted to the distal end of the serial chain. Since we do not restrict the interaction between a robot and the object to be limited to the end-effector, we use the term *effector* to refer to any link or surface on the robot that contacts the object. Multi-effector grasps are potentially superior to finger-tip or end-effector grasps because they allow the robot arms to envelop the object. Such *enveloping grasps* result in superior stability and better robustness. Secondly, the grasped object can be quite large: it can be comparable to the size of the manipulator.

In order for robots to cooperatively manipulate an object, coordinated dynamic control is very important. When two or more robot arms contact the same object, one or more closed kinematic chains are formed. This system is kinematically and dynamically constrained and, in general, extremely nonlinear and coupled. The contact between the arm and the object may include surface rolling and sliding, which introduces nonholonomic and unilateral constraints. Quite often these systems have redundancy in actuation which must be addressed.

Dual arm manipulation [11, 22, 17, 27, 44, 54, 50], multi-fingered grasping [4, 10, 14, 24, 51], and legged locomotion [18, 30] have been studied extensively. A comprehensive account of research on coordinated motion control of multiple robot arms or fingers has been presented in [17]. However, the focus in most of these papers is on the control of mechanical systems with closed kinematic chains. There has been very little emphasis on the modeling of the contact interactions and control of the contact conditions. It is commonly assumed in many papers [12, 48, 35, 41, 43, 46, 47, 50] that each robot grasps the object with an end-effector in such a way that conditions for *form closure* are satisfied at each end-effector. In other words, the contact constraints are maintained regardless of the forces and moments acting at the contact. Further, there is no relative motion between the robot arm and the object. This is only a very *special* case of dual arm manipulation.

When the object is awkwardly shaped and its size is large compared to that of the effectors, the effectors must exert appropriate contact forces to sustain the condition of *force closure*. In this regard, the robots act as *distributed* effectors [37, 45]. Although the dynamic control problem for holonomic systems has been studied, there has been much less emphasis on control of systems in which the constraints are unilateral and nonholonomic. The kinematics of the constraints and the implications on the control of such systems have been studied in literature on multi-fingered grasping [14, 38] and multi-legged walking [21, 30], but dynamic control has not been discussed. Kinematic models of sliding and rolling have been developed [2, 24, 28]. The control of nonholonomic systems is investigated in [6, 7, 39]. Control of sliding has been studied in [3] with the assumption that pure rolling never occurs. The problem of static indeterminacy (redundancy), and optimal solutions of the problem of distribution of forces have been studied for multi-fingered gripers [14, 24, 8, 10, 24, 20, 51] and for legged locomotion systems [30, 16, 18, 21]. In most previous studies, the redundancy in actuation is resolved through an *ad hoc* scheme such as a pseudo-inverse decomposition [38]. The problem of controlling the interaction between manipulators at the contact has been largely ignored in this body of theory.

In this paper, the planning and dynamic control of systems with unilateral constraints (including frictional constraints) is addressed. The focus is on controlling rolling contacts in manipulation and

on planning optimal rolling motion in order to adapt a multi-effector grasp to external forces and to the trajectory. Two planar 3-R manipulators and a two-effector grasp are used to study the underlying problems and to demonstrate the basic ideas. The geometry is deliberately chosen to be simple so that complexity of the nonlinear rigid body dynamics does not obscure the key research issues: control of rolling contact conditions and planning of adaptive rolling motion. The example does not over simplify the problem: the system is governed by kinematic and dynamic constraints due to the closed chain structure, the unilateral constraints at the contacts are preserved, and actuator forces (torques) are underdetermined due to redundancy in actuation.

The mathematical modeling of three-dimensional, multi-effector, enveloping grasps is presented in Section 2. This includes the kinematics and the dynamic equations of motion. The exact form of the equations are presented for the two-effector planar grasp. The control of unilateral systems is discussed in Section 3. The simultaneous force and motion control problem is formulated and the nonlinear feedback for the system is derived. The planning of the rolling motion and the choice of force set-points is discussed in Section 4. Results from a computer simulation of two planar 3-R manipulators and experimental results on two cooperating PUMA 250 manipulators are presented in Section 5. Finally, a summary of the work and plans for future work are discussed in Section 6.

2   Modeling and Problem Formulation

2.1   Notation

We consider l contacts with the object at the points P_1 through P_l. O_k (position vector $r_{O,k}$) is the point fixed to the object such that it is instantaneously at P_k while E_k (position vector $r_{E,k}$) is the point on the effector, instantaneously coincident with P_k as shown in Figure 1. The positions of these three points are the same, but in general, their velocities (and accelerations) are different. r_O is the position of the origin of the object-fixed reference frame which is located at the center of mass, C. In this paper the components of a vector, unless otherwise specified, will be expressed in a global, fixed reference frame.

A robot has n links with a coordinate system attached to each of its links. The origin of the coordinate system for link j on robot i is at A_{ij}. The corresponding position vector is r_{ij} (which is an abbreviation for $r_{A,ij}$). Unless otherwise specified and whenever the context is appropriate, a subscript ij refers to the point A_{ij} and the subscript ij,k refers to the point P_k on the jth link on the ith robot. The subscript O (E) refers to the object (effector).

We use p_O to denote a 6 × 1 vector which describes the position and orientation of the object. Clearly p_O is a function of six coordinates:

$$p_O = p_O(x_O, y_O, z_O, \theta_O, \phi_O, \psi_O)$$

where (x_O, y_O, z_O) are the coordinates of the reference point C in the fixed frame (or the components of the vector r_O), and $(\theta_O, \phi_O, \psi_O)$ are the Euler angles that describe the orientation of the object. We prefer the vector representation:

$$p_O = \begin{bmatrix} r_O \\ \mu_O \end{bmatrix}$$

where μ_O is a 3 × 1 vector of *quasi-coordinates*[1] that describe the orientation of the object. The quasi-coordinates are defined so that the angular velocity of the object, ω_O, is given by:

$$\omega_O = \dot{\mu}_O$$

---

[1]See [34] for the definition of quasi-coordinates.

Figure 1: Illustration of notations.

In the planar case, μ_O is a single element, the angular orientation of the object in the plane.

Similarly, p_{ij} is a 6-dimensional vector which describes the position and orientation of link j of robot i:

$$p_{ij} = \begin{bmatrix} r_{ij} \\ \mu_{ij} \end{bmatrix}$$

where the angular velocity of link j of robot i, ω_{ij}, is equal to $\dot{\mu}_{ij}$, and μ_{ij} is the vector of three quasi-coordinates.

v_O and v_{ij} are the linear velocities of point C on the object and the point A_{ij} on link j of robot i respectively. Thus the 6-dimensional velocity vectors can be defined as:

$$\dot{p}_O = \begin{bmatrix} v_O \\ \omega_O \end{bmatrix} \qquad \dot{p}_{ij} = \begin{bmatrix} v_{ij} \\ \omega_{ij} \end{bmatrix}$$

The joint variables for robot i are denoted by $\theta_i = [\theta_{i1}...\theta_{in}]^T$. The Jacobian matrix that relates the velocities of the jth link on the ith robot to its joint velocities is given by J_{ij}. Thus,

$$p_{ij} = p_{ij}(\theta_i); \quad \dot{p}_{ij} = J_{ij}\dot{\theta}_i; \quad \ddot{p}_{ij} = J_{ij}\ddot{\theta}_i + \dot{J}_{ij}\dot{\theta}_i. \tag{1}$$

Note that if the jth link is not the most distal link, the columns in the matrix J_{ij} with indices greater than j will be zero.

The 6×1 velocity vector for link j of robot i can be referred to the contact point (P_k) instead of the point A_{ij}. The vector referred to P_k consists of the angular velocity of the link and the linear velocity of the point P_k on the link, and is given by

$$\Gamma_{E,k}\dot{p}_{ij}$$

3

where

$$\Gamma_{E,k} = \begin{bmatrix} I_3 & -R_{E,k} \\ 0_3 & I_3 \end{bmatrix},$$

I_3 and 0_3 are the 3×3 identity and zero matrices, and $R_{E,k}$ is the skew-symmetric matrix corresponding to the vector $\rho_{E,k} = r_{E,k} - r_{ij}$

$$R_{E,k} = \begin{bmatrix} 0 & -\rho_{E,k,z} & \rho_{E,k,y} \\ \rho_{E,k,z} & 0 & -\rho_{E,k,x} \\ -\rho_{E,k,y} & \rho_{E,k,x} & 0 \end{bmatrix}$$

Similarly, $\Gamma_{O,k}$ transforms the 6×1 vector of object velocities so that it can be referred to the contact point, P_k:

$$\Gamma_{O,k}\dot{p}_O$$

where

$$\Gamma_{O,k} = \begin{bmatrix} I_3 & -R_{O,k} \\ 0_3 & I_3 \end{bmatrix},$$

$R_{O,k}$ is the skew-symmetric matrix corresponding to the vector $\rho_{O,k} = r_{O,k} - r_O$. We also define the matrix Γ_k:

$$\Gamma_k = \Gamma_{E,k}^{-1}\Gamma_{O,k}$$

Then, the velocities of the effector and that of the object are related by

$$\Gamma_{E,k}\dot{p}_{ij} = \Gamma_{O,k}\dot{p}_O - \begin{bmatrix} v_{ij,rel} \\ \omega_{ij,rel} \end{bmatrix} \tag{2}$$

where $\omega_{ij,rel} = \omega_O - \omega_{ij}$ is the relative angular velocity between the contacting bodies and $v_{ij,rel}$ is the relative velocity at the point of contact on link j (robot i). A systematic approach to the derivation of these equations can be found in [28, 2]. Since we are considering rolling contacts only, $v_{ij,rel}$ is equal to zero.

The acceleration equations can be obtained from differentiating Equation (2). They can be written in the form:

$$\ddot{p}_{ij} = \Gamma_{E,k}^{-1}\Gamma_{O,k}\ddot{p}_O + g_i = \Gamma_k\ddot{p}_O + g_i \tag{3}$$

where g_i is a nonlinear function[2] of the relative velocities between the two contacting bodies and the local geometry (up to third order) of each contacting body.

The contact force, f_k, and moment, m_k about the contact point (P_k) exerted by the effector on the object are denoted by the 6-dimensional vector $F_{P,k}$

$$F_{P,k} = \begin{bmatrix} f_k \\ m_k \end{bmatrix}$$

If the kth contact occurs on the jth link of the ith robot, it is convenient to refer the contact force and moment vector to the point A_{ij}, denoted by $F_{ij,k}$. The vector $F_{ij,k}$ consists of the contact forces at the kth contact and the moments about the origin A_{ij}, and is related to $F_{P,k}$ by a transformation:

$$F_{ij,k} = \Gamma_{E,k}^T F_{P,k} \tag{4}$$

Similarly, $\Gamma_{O,k}^T$ transforms $F_{P,k}$ into a vector of contact forces and moments about the reference point C.

$$F_{C,k} = \Gamma_{O,k}^T F_{P,k}$$

---

[2]The exact form of these equations is given in Reference [2].

2.2 Dynamic equations of motion

The equations of motion for each n degree of freedom manipulator can be written in the joint space in the form

$$D_i \ddot{\theta}_i + b_i + \sum J_{ij}^T \Gamma_{E,k}^T F_{P,k} = \tau_i \tag{5}$$

where D_i is the $n \times n$ inertia matrix in the joint space, b_i is a vector of nonlinear functions of the velocity and position, and τ_i is the vector of joint torques. Note that the summation of $J_{ij}^T \Gamma_{E,k}^T F_{P,k}$ includes all values of k which corresponds to contacts on the ith arm and only those j (link j of robot i) for which there exists a contact.

The equations of motion for the object with l contacts can be written as:

$$D_O \ddot{p}_O + b_O = \sum_{k=1}^{l} \Gamma_{O,k}^T F_{P,k} + W \tag{6}$$

D_O is the 6×6 inertia matrix of the object given by

$$D_O = \begin{bmatrix} m_O I_3 & 0_3 \\ 0_3 & M_O \end{bmatrix}$$

where m_O is the mass and M_O is the inertia tensor (along principal axes about the center of mass C) of the object. W is the vector of external forces and moments acting on the object and b_O is a 6-dimensional vector of nonlinear velocity dependent terms:

$$b_O = \begin{bmatrix} 0 \\ \omega_O \times M_O \omega_O \end{bmatrix}$$

The mobility for a holonomic system is the minimum number of independent generalized coordinates required to describe the configuration of the system. If the mobility is m, the task space (or the operational space [15]) is described by an m-dimensional vector of generalized coordinates, ζ. Equations (5-6) can be rewritten as m equations of motion in the task space of the form:

$$\ddot{\zeta} = f(\zeta, \dot{\zeta}) + g(\zeta)\tau \tag{7}$$

Further, if λ is the vector of contact forces in the system, it can be written in the form:

$$\lambda = [F_{P,1} \quad F_{P,2} \quad \cdots \quad F_{P,l}]^T = a(\zeta, \dot{\zeta}) + b(\zeta)\tau \tag{8}$$

This is illustrated with the help of a planar example next.

2.3 Example with two planar 3-R manipulators

Consider two 3-R (three revolute joints) manipulators each making one contact with the manipulated object ($l = 2$) on the $3rd$ link as shown in Figure 2. The most distal link on each arm is shaped so that it has a palmar surface at the end. Since there is only one contact on each arm ($i = k$) and since contact occurs only on the most distal link (j is fixed at 3), we simplify the notation. Denote p_{i3} by p_i, J_{i3} by J_i, and the contact force $F_{P,i}$ by F_i. Note that

$$\theta_i = [\theta_{i1} \quad \theta_{i2} \quad \theta_{i3}]^T \qquad \qquad \tau_i = [\tau_{i1} \quad \tau_{i2} \quad \tau_{i3}]^T$$

$$\Gamma_{O,1} = \begin{bmatrix} 1 & 0 & -\rho_{O,1,y} \\ 0 & 1 & \rho_{O,1,x} \\ 0 & 0 & 1 \end{bmatrix} \qquad \qquad \Gamma_{E,1} = \begin{bmatrix} 1 & 0 & -\rho_{E,1,y} \\ 0 & 1 & \rho_{E,1,x} \\ 0 & 0 & 1 \end{bmatrix}$$
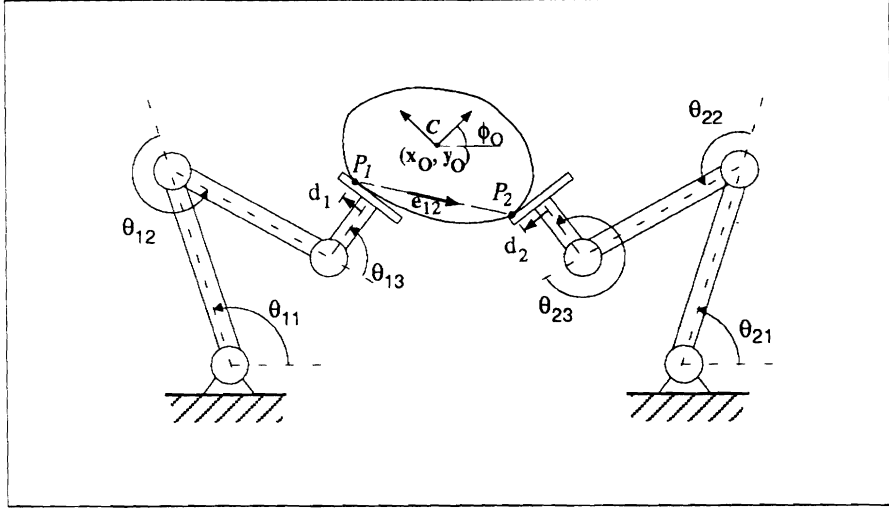
5

Figure 2: Two robot arms manipulating an object.

If rolling contact is maintained the mobility of the system is 5. Therefore ζ may be chosen to consist of 3-dimensional p_O and two other independent position variables. Since the objective is to control the rolling contact, we choose two contact configuration variables [52]. The point of contact on the ith palm is described by the contact coordinate d_i which is the arc-length along the palm as shown in Figure 2. Thus the task space can be defined by p_O, d_1 and d_2. However, in general, it is difficult to derive closed form expressions for d_i in terms of the joint angles. Therefore we choose the orientation of the two palmar surfaces, ϕ_1 and ϕ_2 respectively, as the two other generalized coordinates:

$$\phi_1 = \theta_{11} + \theta_{12} + \theta_{13} \qquad \phi_2 = \theta_{21} + \theta_{22} + \theta_{23}$$

Thus, the task space variable ζ is:

$$\zeta = \begin{bmatrix} p_O^T & \phi_1 & \phi_2 \end{bmatrix}^T = \begin{bmatrix} x_O & y_O & \phi_O & \phi_1 & \phi_2 \end{bmatrix}^T$$

The dynamic equations of motion for the manipulators in the joint space are given in Equation (5). The motion equations of the ith manipulator ($i = 1, 2$) in the task space can be derived [42] by eliminating $\ddot{\theta}_i$ from Equation (1) and Equation (5) and simplifying:

$$H_i \ddot{p}_i + h_i + \Gamma_{E,i}^T F_i = J_i^{-T} \tau_i \tag{9}$$

where

$$H_i = J_i^{-T} D_i J_i^{-1}$$

and

$$h_i = -J_i^{-T} D_i J_i^{-1} \dot{J}_i \dot{\theta}_i + J_i^{-T} b_i.$$

Now since we want to express all equations in the task space (ζ), we substitute Equation (3) into Equation (9) to get

$$H_i \Gamma_i \ddot{p}_O + (H_i g_i + h_i) + \Gamma_{E,i}^T F_i = J_i^{-T} \tau_i \tag{10}$$

From Equations (6) and (10), we obtain

$$\ddot{p}_O = U^{-1} \Lambda \tau + U^{-1} W - U^{-1} \Gamma^T \begin{bmatrix} H_1 g_1 + h_1 \\ H_2 g_2 + h_2 \end{bmatrix} - U^{-1} b_O \tag{11}$$

6

where

$$U = D_O + \Gamma_1^T H_1 \Gamma_1 + \Gamma_2^T H_2 \Gamma_2, \qquad \tau = [\tau_1^T \quad \tau_2^T]^T, \qquad \Gamma = [\Gamma_1^T \quad \Gamma_2^T]^T,$$

and

$$\Lambda = [\Gamma_1^T J_1^{-T} \quad \Gamma_2^T J_2^{-T}].$$

Note that U is the task space inertia of the complete system.

The contact forces and moments can easily be calculated. For example, the expression for F_1 is obtained by substituting Equation (11) into Equation (10):

$$F_1 = a_1(\zeta, \dot{\zeta}) + b_1(\zeta)\tau \tag{12}$$

where

$$a_1(\zeta, \dot{\zeta}) = (\Gamma_{E,i}^T)^{-1} \left[H_1 \Gamma_1 U^{-1} \Gamma^T \begin{bmatrix} H_1 g_1 + h_1 \\ H_2 g_2 + h_2 \end{bmatrix} - H_1 \Gamma_1 U^{-1} W + H_1 \Gamma_1 U^{-1} b_O - H_1 g_1 - h_1 \right]$$

$$b_1(\zeta) = (\Gamma_{E,i}^T)^{-1} \left[-H_1 \Gamma_1 U^{-1} \Gamma_1^T J_1^{-T} + J_1^{-T} \quad -H_1 \Gamma_1 U^{-1} \Gamma_2^T J_2^{-T} \right]$$

Since φ_i is a function of θ_i, expressions for $\ddot{\phi}_1$ and $\ddot{\phi}_2$ can be derived quite easily. First, the joint accelerations are given by Equation (5):

$$\ddot{\theta}_i = D_i^{-1} \left(\tau_i - b_i - J_{ij}^T \Gamma_{E,i}^T F_i \right) \tag{13}$$

Since

$$\ddot{\phi}_i = \ddot{\theta}_{i1} + \ddot{\theta}_{i2} + \ddot{\theta}_{i3},$$

from Equation (13) we get:

$$\ddot{\phi}_i = \sum_{i=1}^{3} \left(D_i^{-1} \left[\tau_i - b_i - J_{ij}^T \Gamma_{E,i}^T F_i \right] \right) \tag{14}$$

To get $\ddot{\phi}_1$, we can substitute Equation (12) into Equation (14). Similarly, by deriving an expression for F_2 we can get $\ddot{\phi}_2$ from Equation (14). Thus we see that the expressions of the second derivatives of the task space variables are of the form shown in Equation (7). F_1 in Equation (12) is an example of a contact force. The expression is of the form shown in Equation (8).

We note that if the object, for example, is cylindrical with radius R, the contact coordinates d_1 and d_2 can be related to the generalized coordinates on the task space variables ζ:

$$\dot{d}_i = R(\dot{\phi}_O - \dot{\phi}_i)$$

This can be integrated to get

$$d_i = R(\phi_O - \phi_i) + c_i$$

where c_i is a constant that depends on the initial values of d_i, ϕ_O, and ϕ_i.
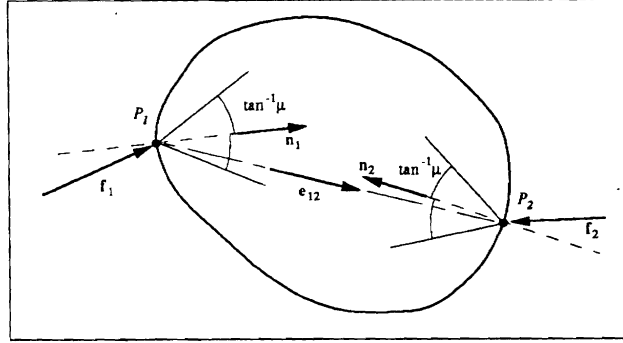
Figure 3: Two-point contact.

2.4 Rolling contact constraints

If we adopt the point-contact model [38], the contact interaction can be modeled by a pure force through the contact point. Therefore, the moments (m_k) in the 6-dimensional vector, $F_{P,k}$, are equal to zero, and the contact interaction can be modeled by a pure force vector, f_k. In the planar example considered in Figure 2, f_k lies in the plane.

There are two types of constraint conditions that must be satisfied for rolling. Firstly, the component of force along the inward pointing normal must be nonnegative to maintain contact. If n_i is the inward pointing normal for the object at the contact point P_i as shown in Figure 3, we have the condition:

$$f_i \cdot n_i \geq 0 \qquad (15)$$

Secondly, the tangential and normal components must be such that the required rolling contact condition is satisfied. If we assume the validity of Coulomb's model of friction, the following equation must be true:

$$|f_i - (f_i \cdot n_i) n_i| \leq \mu f_i \cdot n_i \qquad (16)$$

where μ is the coefficient of friction at the contact.

For two point-contacts, Equation (16) can be satisfied for arbitrary loads and trajectories only if the contact normals, n_1 and n_2, and the unit vector along the line joining P_1 to P_2, e_{12}, satisfy the inequalities:

$$\cos^{-1}(e_{12} \cdot n_1) \leq \tan^{-1}\mu \, ; \quad \cos^{-1}(-e_{12} \cdot n_2) \leq \tan^{-1}\mu \qquad (17)$$

These are necessary and sufficient conditions for being able to maintain force closure in two-point contact grasps [14, 29] regardless of external disturbances. A discussion for more complicated geometries can be found in [18, 29, 38]. If the strict inequality holds in Equation (16), the tangential velocities at the two contact points are identical. If the equality condition holds, the contact is rolling if the relative velocity is zero ($v_{i,rel} = 0$), otherwise the contact slips.

3 Controller Design

The objective of the controller is to control the trajectory of the object, and the contact conditions. Since we consider rolling contact, the goal is to maintain rolling, that is, to avoid sliding and separation at each contact point. This implies that the forces must be actively controlled so that they satisfy the inequalities (15) and (16). First we discuss how this can be accomplished, and then develop an algorithm for simultaneously controlling motion and and contact conditions.

3.1 Critical contact force

Each link making contact with the object can only push and cannot pull the object. Additionally, the pushing force must be within the friction cone. It must be built into the controller to avoid separation and slipping at the contact points. In another words, inequalities (15) and (16) must be enforced. This necessitates the control of contact forces f_i. However, we may not have enough actuator inputs to control every contact force as well as the motion trajectory variables. For a system of mobility m with r actuators, it is possible to control $r - m$ components of contact forces and moments and m position variables. For the two planar 3-R manipulators discussed in the preceding section, the system has six actuators and the mobility is five. In addition to controlling five position variables $(x_O, y_O, \phi_O, \phi_1, \phi_2)$, we can control one force variable. This force variable and its desired value must be chosen to ensure that the inequality constraints are satisfied, and thus the rolling conditions are maintained.

In the previous work, this was accomplished by specifying the internal forces [38, 24] or the interaction force [19]. For planar, two-point contacts as in Figure 2, the finger forces can be decomposed into manipulation forces, $f_{i,m}$ and internal forces, $f_{i,n}$.

$$f_i = f_{i,m} + f_{i,n}$$

The internal forces are equal and opposite forces along e_{12}. Thus,

$$f_{1,n} = -f_{2,n} = \frac{1}{2}f_I = \frac{1}{2}(f_1 - f_2) \cdot e_{12} \tag{18}$$

f_I is called the interaction force [19]. The manipulation forces are computed from the description of the trajectory and external forces/moments. They resist the external forces and produce the desired accelerations. Further, they are required to be such that the norm of the vector $[f_{1,m}^T \quad f_{2,m}^T]^T$ is minimum. As shown in Reference [19], $(f_{1,m} - f_{2,m}) \cdot e_{12} = 0$. From the task description, a suitable value for f_I is computed. The desired trajectory, external forces and the desired interaction force, f_I, specify the force set-points.

In the present approach, the desired interaction force is calculated from the limits on the contact forces — for example, the minimum normal component so that Equation (15) is satisfied with some factor of safety. We adopt a different strategy. We directly control the force component that is closest to its limit. Instead of controlling the interaction force, we control the *critical contact force*, f_{cc}, which is defined as:

$$f_{cc} = \min\{e_{12} \cdot f_1, -e_{12} \cdot f_2\} \tag{19}$$

By specifying the critical contact force, we specify the minimum contact force along e_{12}. The larger this component, the greater the interaction force (and the internal forces). The advantage in controlling the critical contact force is that we explicitly control each individual force component, $f_1 \cdot e_{12}$ and $f_2 \cdot e_{12}$, instead of controlling the difference.

Equation (19) can also be written in the following form

$$f_{cc} = \frac{e_{12} \cdot f_1 - e_{12} \cdot f_2 - \mid e_{12} \cdot f_1 + e_{12} \cdot f_2 \mid}{2} \tag{20}$$

Since this equation is not differentiable due to the presence of absolute value, including f_{cc} in the output equation will make the controller design difficult. In order to circumvent this problem, we include $e_{12} \cdot f_1$ in the output equation. In Appendix A, we show that by controlling $e_{12} \cdot f_1$, the error in f_{cc} is bounded.

9

3.2 Simultaneous control of trajectory and contact conditions

In order to perform the task of manipulating the object by multiple arms, the controller must regulate the position and orientation of the object, and the contact conditions. The control of the contact conditions necessities the control of certain forces, *e.g.*, the critical contact force for the two 3-R manipulators discussed in the previous subsection. In this subsection, we present a method for simultaneous control of motion trajectory and forces.

In earlier papers [53, 33, 31], we have demonstrated the advantage of *dynamic* state feedback. We have rigorously shown that an integral feedback is needed to stabilize force control systems. Applying differential geometrical control theory [13], we have also been able to find a nonlinear dynamic state feedback which *exactly linearizes* and *completely decouples* the position control loop and force control loop. This allows us to design each subsystem by using linear system theory.

The dynamic state feedback is realized by including the joint torques τ as part of the state variable, or equivalently, by introducing an integrator on each input channel:

$$x = [x_1 \quad x_2 \quad x_3]^T = [\zeta \quad \dot\zeta \quad \tau]^T$$

Now, Equation (7) can be rewritten in the state space

$$\dot{x} = \begin{bmatrix} \dot{x}_1 \\ \dot{x}_2 \\ \dot{x}_3 \end{bmatrix} = \begin{bmatrix} x_2 \\ f(x_1,x_2) + g(x_1)x_3 \\ 0 \end{bmatrix} + \begin{bmatrix} 0 \\ 0 \\ I \end{bmatrix} u$$
$$= \xi(x) + \eta(x)u \tag{21}$$

while the output equations have the form

$$y = \begin{bmatrix} y_1 \\ y_2 \end{bmatrix} = \begin{bmatrix} x_1 \\ E(x_1)^T (a(x_1,x_2) + b(x_1)x_3) \end{bmatrix} \tag{22}$$

where y_1 is an $m \times 1$ function of position and y_2 an $(m-r) \times 1$ function of constraint forces. $E(x_1)$ is a projection matrix that depends on the choice of y_2. For example, in the planar system in Figure 2, the outputs are given by

$$y = \begin{bmatrix} y_1 \\ y_2 \end{bmatrix} = \begin{bmatrix} x_1 \\ e_{12}^T F_1 \end{bmatrix} = \begin{bmatrix} x_1 \\ e_{12}^T [a(x_1,x_2) + b(x_1)x_3] \end{bmatrix} \tag{23}$$

In [53] we propose a nonlinear feedback which linearizes and decouples the nonlinear system represented by Equations (21) and (22). The feedback has the form:

$$u = \alpha(x) + \beta(x)v \tag{24}$$

where $\alpha(x)$ and $\beta(x)$ are to be constructed based on the system model. Using differential geometric design techniques [13] for nonlinear systems, $\alpha(x)$ and $\beta(x)$ can be found by solving the following matrix equations [53]

$$\Phi(x)\alpha(x) = -\begin{bmatrix} L_\xi^3 y_1 \\ L_\xi y_2 \end{bmatrix} \quad ; \quad \Phi(x)\beta(x) = I \tag{25}$$

where $\Phi(x)$ is the decoupling matrix of the system which is given by

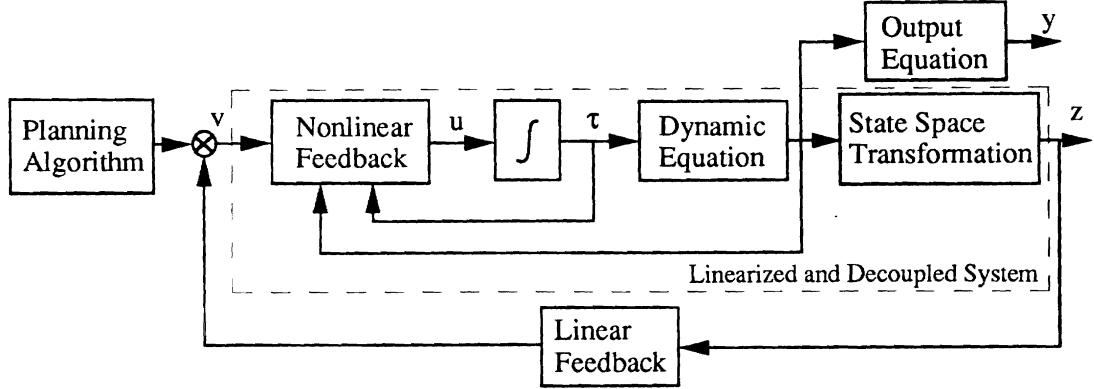$$\Phi(x) = \begin{bmatrix} L_\eta L_\xi^2 y_1 \\ L_\eta y_2 \end{bmatrix}$$

Figure 4: Schematic of the Nonlinear feedback control algorithm.

Here $L_\xi y_i$ is the Lie derivative of y_i along the vector field ξ:

$$L_\xi y_i = \frac{\partial y_i}{\partial x} \xi$$

In the case of two 3-R manipulators, u, α and v are 6-dimensional vectors, and β and Φ are 6×6 matrices.

Application of the above feedback linearizes the system in a transformed state space z. The new state variable z, and x are related by [13]:

$$z = [z_1 \quad z_2 \quad z_3 \quad z_4]^T = [y_1 \quad L_\xi y_1 \quad L_\xi^2 y_1 \quad y_2] \tag{26}$$

The linearized system is characterized by

$$\begin{bmatrix} \dot{z}_1 \\ \dot{z}_2 \\ \dot{z}_3 \\ \dot{z}_4 \end{bmatrix} = \begin{bmatrix} 0 & I & 0 & 0 \\ 0 & 0 & I & 0 \\ 0 & 0 & 0 & 0 \\ 0 & 0 & 0 & 0 \end{bmatrix} \begin{bmatrix} z_1 \\ z_2 \\ z_3 \\ z_4 \end{bmatrix} + \begin{bmatrix} 0 & 0 \\ 0 & 0 \\ I & 0 \\ 0 & I \end{bmatrix} \begin{bmatrix} v_1 \\ v_2 \end{bmatrix} \tag{27}$$

and the output equation is given by

$$\begin{bmatrix} y_1 \\ y_2 \end{bmatrix} = \begin{bmatrix} I & 0 & 0 & 0 \\ 0 & 0 & 0 & I \end{bmatrix} \begin{bmatrix} z_1 \\ z_2 \\ z_3 \\ z_4 \end{bmatrix} \tag{28}$$

We note that position control subsystem is third order while the force control subsystem is first order. A schematic of the control algorithm is shown in Figure 4. The system shown within the dotted line is linear and decoupled.

A linear feedback can be further designed to place the poles of the system at appropriate locations to achieve the desired performance requirements.

4 Planning Rolling Contact Motion

In this section, we consider the planning of the rolling motion at each contact. The discussion is restricted to planar geometries with two point-contacts. We assume that the trajectory of the

11

manipulated object is specified. However, the trajectory of the system is not completely specified. For example, if we consider the geometry shown in Figure 2, we assume that the trajectory of the object, $p_O(t)$ is specified. However, the rolling motion $d_1(t)$ and $d_2(t)$ (and therefore, $\phi_1(t)$ and $\phi_2(t)$) is not specified. Note that this is different from traditional path planning or motion planning (see for example References [26, 25, 9, 23]) in which the goal is to find a feasible or optimal path between two given positions. Here the trajectory is provided to us. Since this does not uniquely specify the motion of the system, there is an opportunity to plan an appropriate rolling motion that will adapt the grasp to the external forces and the trajectory.

Since the contacts may change (due to the rolling motion) during the task, it is meaningful to plan the trajectory of the contact points in order to maximize, or keep a preferred stability index within reasonable limits. On the other hand, it is also beneficial to locate the contacts so that the actuator forces for a given load and object trajectory are minimal.

The simple two-dimensional example with a circular object in Figure 5 illustrates this. Let f_r (m_r) be the resultant force (moment about the center of mass) on the object that is required to oppose the external forces (including the gravitational force) and the inertial forces. The inertial forces can be obtained from the trajectory and the inertial properties of the object. Thus we have the equations:

$$f_r = f_1 + f_2 \tag{29}$$

$$m_r = \rho_{O,1} \times f_1 + \rho_{O,2} \times f_2 \tag{30}$$

where f_1 and f_2 are forces applied to the object by the two palms respectively.

Suppose the dominant force is the weight (pointing down) so that, in Equations (29) and (30), $f_r = -W$ and $m_r = 0$. In Figure 5(a), the two palms face each other and n_1 and n_2 are colinear but in opposite directions. Clearly, the inequalities in Equation 17 are satisfied. If the contact forces are not limited, by pushing sufficiently hard, the exerted forces f_1 and f_2 can always be kept within the friction cone while opposing the weight W. This configuration is robust to small changes in W: the critical contact force can be increased to satisfy the friction cone constraints. However, the object may not be able to withstand a large contact force and/or the large forces f_1 and f_2 required may be beyond the torque limits of the manipulators.

The other extreme case occurs when the two contact points coincide (see Figure 5(b)). n_1 and n_2 are again colinear but now, they have the same direction. The inequalities in Equation 17 are violated. Although the external force W can be resisted most efficiently (with the smallest actuator forces) in this configuration, changes in the direction of W (perhaps caused by external disturbances) cannot be compensated by f_1 and f_2.

The grasp in Figure 5(a) results in large contact forces but a more robust grasp because the vector e_{12} is "centered in each friction cone". On the other hand, the grasp in Figure 5(b) requires relatively smaller contact forces but the grasp is quite sensitive to external disturbances because e_{12} is outside both friction cones[3].

Thus, if the weight is the only external force, it is meaningful to roll from the configuration in Figure 5(a) to the one that is close to Figure 5(b). On the other hand, if disturbing forces (say in the horizontal direction) are expected, the configuration in Figure 5(a) is better. In general, there is a trade-off between these two conflicting requirements of *lower actuator forces* (superior mechanical advantage) and *robustness* (greater resistance to slippage).

We now develop an algorithm which plans the motion on the contact surface so that the force applied to the object by each palm is centered within the *contact friction cone*, thereby decreasing

---

[3]Actually, e_{12} cannot be defined in the limiting case shown in Figure 5(b) but if we examine the case in which the two contact points are close to one another but not coincident, then it is obvious that e_{12} is outside the friction cones.
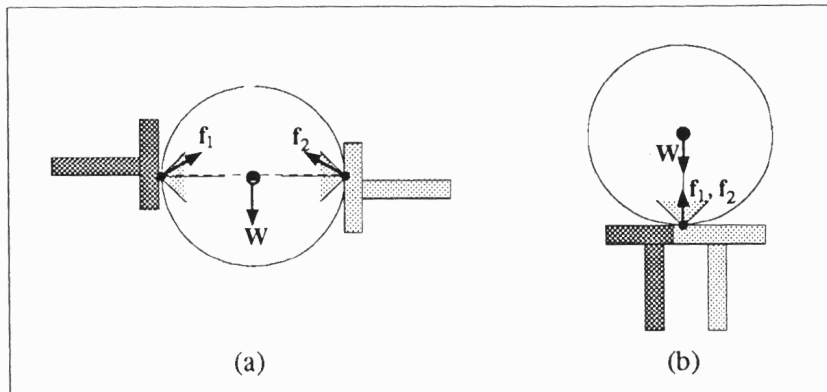
Figure 5: Palm contact locations.

the possibility of violating the constraint in Equation (16). This planner will then function as an input to the control system when a specified task is to be performed. For the sake of simplicity, we consider flat effectors (palms) and a convex, smooth object. The basic idea is to specify the relative importance of better robustness versus low actuator forces (higher mechanical advantage) by specifying the critical contact force. As shown below, this also determines the optimal location of the contact points.

Consider the general case where n_1 and n_2 are not colinear as shown in Figure 3 and f_r and m_r are quite general. Let the contact point on the object, P_i, have the arc-length coordinate (or the contact coordinate) s_i. It is clear that the normals and the vector e_{12} are functions of the contact points:

$$n_i = n_i(s_i); \qquad e_{12} = e_{12}(s_1, s_2)$$

In order to minimize the tendency to slip it is necessary to minimize the maximum frictional angle. This is accomplished when the two friction angles are equal, and further, made equal to zero. In other words, f_i should be along the normal n_i. The equilibrium equations for the object (Equations (29) and (30)) are:

$$\|f_1\|n_1(s_1) + \|f_2\|n_2(s_2) = f_r \tag{31}$$

$$\rho_{O,1}(s_1) \times \|f_1\|n_1(s_1) + \rho_{O,2}(s_2) \times \|f_2\|n_2(s_2) = m_r \tag{32}$$

As before, f_r and m_r include not only external forces and moments acting on the object but also the inertial forces and moments. Let the desired (specified) critical contact force be f_{cc}^d. Without loss of generality, designate the critical contact point to be P_1. Now we have the requirements

$$f_1 \cdot e_{12}(s_1, s_2) = f_{cc}^d \tag{33}$$

$$f_2 \cdot e_{12}(s_1, s_2) \geq f_{cc}^d \tag{34}$$

Thus, for a given load (f_r and m_r), the ideal set of contact points and contact forces should be such that Equations (31), (32), (33), and (34) should be satisfied. This reduces to solving the four equations for s_1, s_2, f_1, and f_2. Although these are nonlinear equations, a solution should, in general, be possible.

However, such a solution cannot be found for the special case of cylindrical objects, unless $m_r = 0$. If $m_r = 0$, because Equation (32) is automatically satisfied for any s_1 and s_2, there are infinite solutions to this problem. If we further assign the two arms to share the load equally we
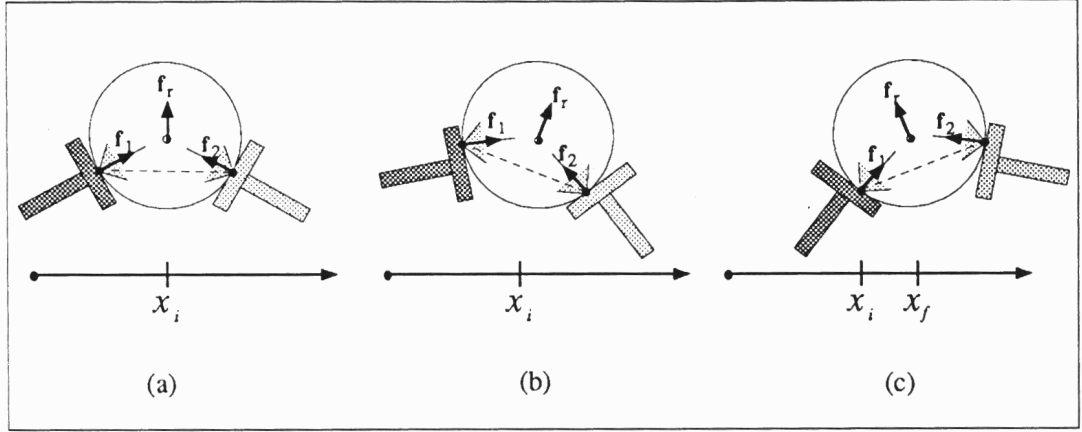
13

Figure 6: Manipulation with rolling contacts.

obtain a unique solution. In order for the friction angle to be equal, the two contact force vectors must form the same angle with f_r as shown in Figure 6. The components of f_1 and f_2 along f_r will be one half the magnitude of f_r (equal load-sharing) while the projections along e_{12} are equal to the desired critical contact force, f_{cc}^d.

Figure 6 shows a sequence of two arms moving along a trajectory from x_i to x_f. At x_i (Figure 6(a)) the arms merely hold the object and support its weight. As the object is moved from x_i (Figure 6(b)), the inertial forces change the direction of f_r. The contact points are moved *via* a rolling motion to the optimal locations shown in the figure. In the final segment of the trajectory (close to x_f), the two palms decelerate the object (Figure 6(c)). Once again the contacts are adapted to the trajectory and the changing forces.

This section described the basic philosophy behind the planning motion to adapt the grasp configuration to the changing trajectory and external load. Although the basic ideas are applicable to more complicated geometries as well, the nonlinear equations in Equations (31,32,33) are difficult to solve analytically. Computer simulation and experimental results on such a strategy are described in the next section.

5 Simulations and Experiments

Both computer simulations and physical experiments have been performed to verify the control and planning algorithms developed in the preceding sections. The manipulation task chosen in the simulation and experiment is to move a circular object (a soccer ball in the experiment) horizontally in an oscillation over a distance of 0.4 meters with a specified period T_m. The desired trajectory in the horizontal x-direction is a sinusoid given by

$$x_O^d(t) = x_{O,init} + 0.2 \left[\sin \left(\frac{2\pi}{T_m} t - \frac{\pi}{2} \right) + 1.0 \right] \tag{35}$$

where $x_{O,init}$ is the desired initial value of x_O. The desired trajectories $y_O^d(t)$ and $\phi_O^d(t)$ are constant over time. The planned values for ϕ_1 and ϕ_2 are calculated by the planning algorithm as described in Section 4. The desired value for the critical contact force f_{cc}^d is also chosen to be a constant. The linear feedback in Figure 4 is chosen so that the third order position control subsystem has all the three poles at at $s = -10$ and the first order force control subsystem has its pole at $s = -10$.

14

5.1 Simulation results

The simulation is conducted by using kinematic and dynamic models of PUMA 250s. This is the same model on which the feedback control algorithm used in the experiment is based. A global coordinate system is chosen at the base of robot 1. All the position and orientation parameters described below are relative to the global coordinates. The bases of the two robots are separated by a distance equal to 0.4 meters. The key kinematic and dynamic parameters are included in Appendix B.

The simulation results are shown in Figures 7 through 9. The position trajectories of the object are shown in Figure 7. The desired trajectory of x_O is given by (35) with $x_{O,init} = 0.0$ and $T_m = 4.0$ seconds while the desired value of y_O is 0.3. Figures 7(a) and 7(b) illustrate the actual trajectories of x_O and y_O while Figure 7(c) displays the errors in x_O and y_O. It is seen that the errors vanishes within one second. The maximum error in x_O is about 1.8 mm and that in y_O is about 4.3 mm.

The trajectories for the orientation, ϕ_1 and ϕ_2, of the two palms are illustrated in Figure 8. The planned values for ϕ_1 and ϕ_2, shown by dashed line, are computed using the planning algorithm discussed in Section 4 (and are therefore called "planned" values rather than "desired" values). The goal of orienting the palms is to adapt the contact configuration as to keep the contact forces within the friction cone. The actual trajectories of ϕ_1 and ϕ_2 are shown in solid line. It is clear that, while both arms consistently follow the planned trajectories, there is a constant lag in the response. Since the position control subsystems are of third order (Equations (27) and (28)), the controller requires the desired values of the position output variables as well as their desired first and second order derivatives. The derivatives of the desired trajectory ($\dot{x}_O^d$, $\dot{y}_O^d$, $\dot{\phi}_O^d$, $\ddot{x}_O^d$, $\ddot{y}_O^d$, $\ddot{\phi}_O^d$) are easily calculated. Thus, x_O and y_O perfectly track the desired trajectories after the initial transient. However, the derivatives of ϕ_1 and ϕ_2 are not calculated by the planning algorithm. This is because the planned rolling motion depends on the inertial and external forces. The inertial forces are functions $\ddot{x}_O$, $\ddot{y}_O$, $\ddot{\phi}_O$, ϕ_1 and ϕ_2, and the velocities. If the planned motion $\phi_1(t)$ and $\phi_2(t)$ is to depend on the inertial forces and moments, we have a paradoxical situation in which $\phi_1(t)$ and $\phi_2(t)$ depend on $\ddot{\phi}_1$ and $\ddot{\phi}_2$. To avoid this, the planned rolling motion, $\phi_1^d(t)$ and $\phi_2^d(t)$, depends on the external forces and on the inertial forces estimated from $\ddot{x}_O^d(t)$, $\ddot{y}_O^d(t)$ and $\ddot{\phi}_O^d(t)$. The planning algorithm is "suboptimal" in this sense. However, changes in inertial forces and moments due to variations in the orientations of the palm or changes in contact locations can be expected to be relatively small. The implication of this approach is that the feedforward compensation, that is, the first and second order derivatives of $\phi_1^d(t)$ and $\phi_2^d(t)$, is not provided in the controller. This causes the lag in the response of ϕ_1 and ϕ_2.

Figure 9 depicts the trajectories of the critical contact force f_{cc} and the friction angle of the two contact forces f_1 and f_2. The desired value of f_{cc} is 10.0 Newtons. The actual trajectory of f_{cc} in the simulation exhibits the response that is typical of a first order system, as shown in Figure 9(a). The friction angle of the contact force f_i is the angle between the outward normal of palm i and the direction of f_i. The goal of controlling the rolling motion is to keep the friction angles close to zero, that is, keep the contact force f_i close to the center of the friction cone. It is shown in Figure 9(b) that the friction angles are effectively brought to zero within one second. The initial peak value displayed in Figure 9(b) results from the uncompensated object gravity force at the instant when the simulation is started.
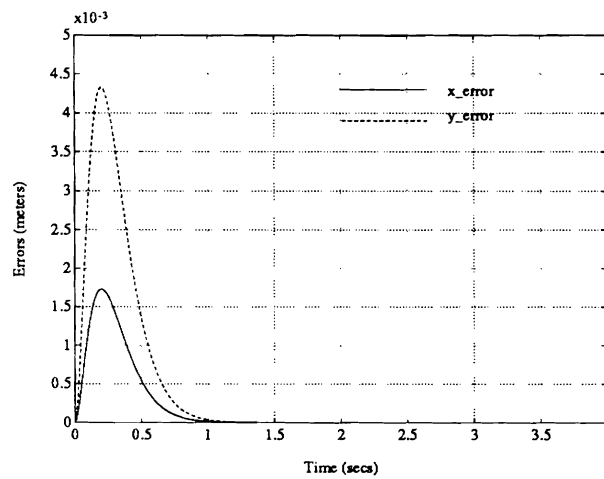
5.2 Experimental results

The control and planning algorithms developed in the previous sections have also been implemented on an experimental system called TRACS (Two Robotic Arm Coordination System) in the
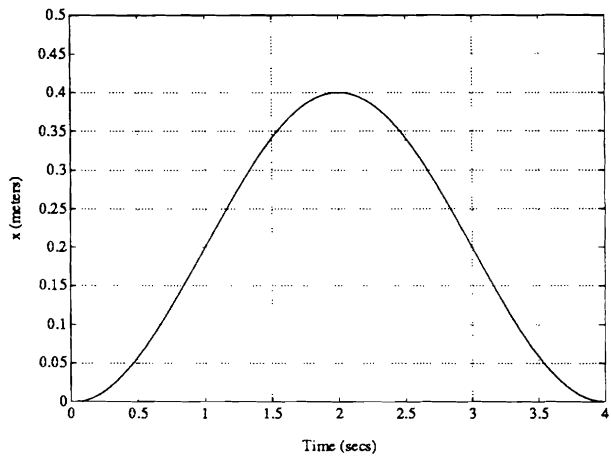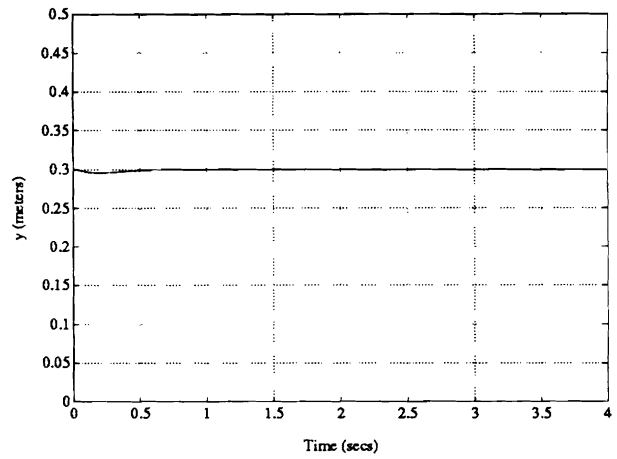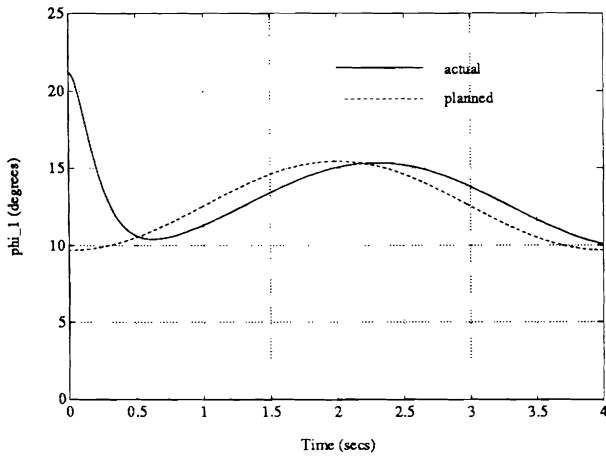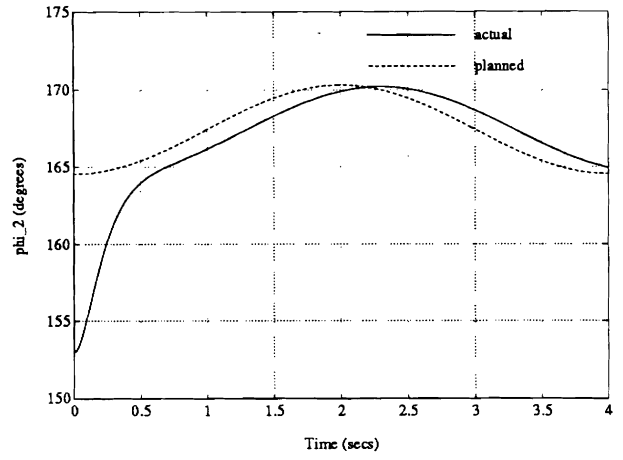
Figure 7: The position trajectories of the object from the simulation: (a) actual x_o, (b) actual y_o, (c) errors in x_o and y_o.
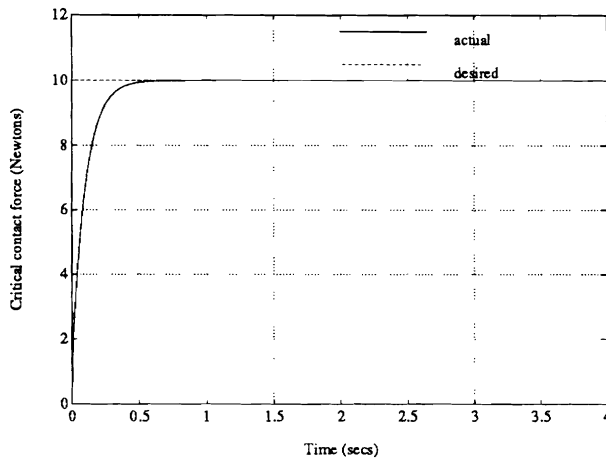
16

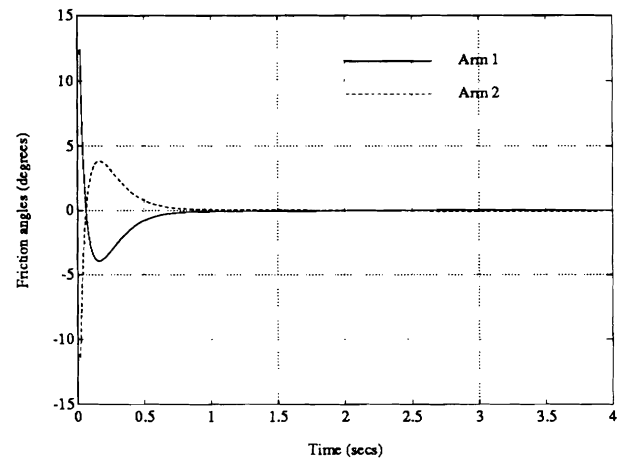(a)   (b)

Figure 8: The planned and actual orientation trajectories of the two arms from the simulation: (a) ϕ_1 of arm 1, (b) ϕ_2 of arm 2.

(a)   (b)

Figure 9: The trajectories of the critical contact force f_{cc} and the friction angles of f_1 and f_2 from the simulation.
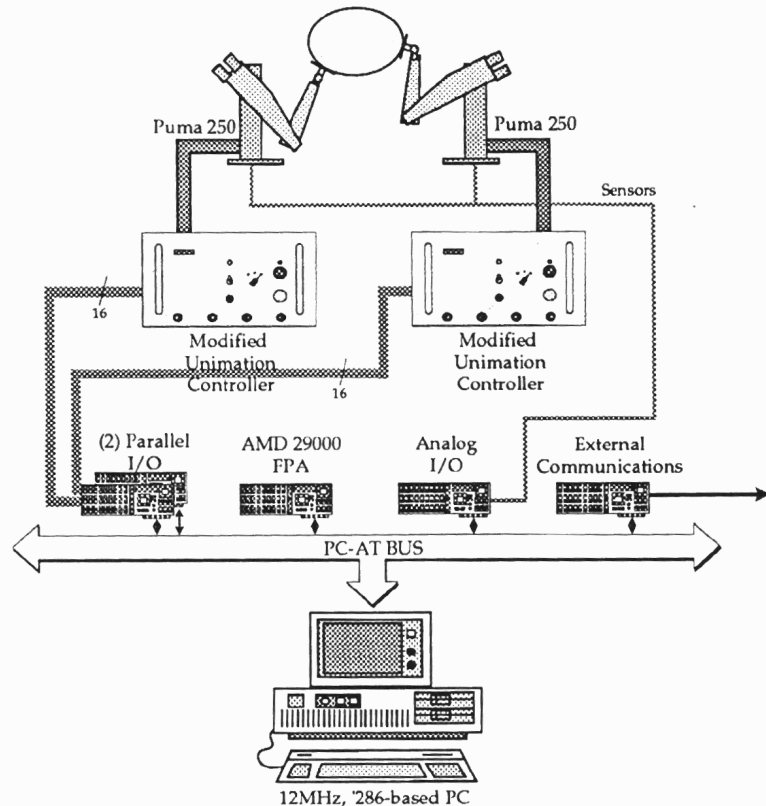
17

Figure 10: The TRACS hardware architecture.

GRASP Laboratory, University of Pennsylvania. The TRACS is exclusively developed for verifying and testing dynamic control algorithms for one arm or two cooperative arms [32]. The hardware architecture of the system is depicted in Figure 10. It consists of two PUMA 250 manipulators. Each manipulator has a flat-surface palm which is instrumented with an Interlink linear tactile sensor. One of the manipulators is equipped with a Zebra six-dimensional force/torque sensor[4]. The system uses a 80286-based IBM PC/AT as the host computer which is aided by an AMD29000 high speed floating point coprocessor. It is configured in such a way that the 80286 processor performs all the I/O interface operations (user interface and sensor/manipulator interface) while the AMD29000 carries out the real-time computations of the control algorithm. The PC/AT has a parallel interface to each PUMA Unimation controller, through which the desired joint torque values are directly written to the DACs (Digital-Analog Converters) and the encoder counts are read back to the PC/AT.

The experimental task is intentionally designed to be the same as the one performed in the simulation. In the experiment, a soccer ball is used as the object to be manipulated. Since the planar motion is considered in the experiment, only three links of the two PUMA 250s (links 2, 3, and 5) are employed. See Appendix B for a detailed sketch of the experimental test-bed. While the manipulators are performing the task of moving the ball back and forth, the readings from the joint encoders, the palm tactile sensors, and the wrist force/torque sensor are recorded in real time.

---

[4]Since there is one force component, $e_{12}^T F_1$, in the output equation, only one force/torque sensor is needed to implement the control algorithm developed in Section 3. In practice, it is preferable to equip both arms with force sensors.

From these readings, the position and orientation of the object, the orientation of the palms, and the critical contact force are computed.

The experiment results are plotted in Figures 11 through 13. Figure 11 shows the desired and actual position of the ball, plus the error trajectories. The system tracks the position trajectory reasonably well. The error in x_o varies within ± 1.0 cm, and that in y_o within ± 1.6 cm.

Figure 12 shows the orientation angles of the two palms. The dashed line is computed from the planning algorithm described in Section 4. It is noted that there is an initial error in the orientation angles. This is because the experiment starts from an initial configuration manually set by the operator, which is in general different from the one calculated by the planning algorithm. Although the overall trend of the orientation is followed, large errors are exhibited in the trajectories of both ϕ_1 and ϕ_2. In spite of these large errors, the contact forces are kept with the friction cone. In fact, the experiment would fail if one of the contact forces fell outside the friction cone.

Figure 13 shows the trajectories of the critical contact force, and the force angle and the friction angle for f_1. The force angle is defined as the angle made by f_1 with the horizontal. The desired value of the critical contact force is 12.0 Newtons. Unlike the smooth response obtained in the simulation, the actual trajectory of the critical contact force shown in Figure 13(a) exhibits substantial variations around the desired value. Since there is only one force/torque sensor available in the experiment (which is installed on robot 1), the information about the contact force f_2 is not available. Figure 13(b) displays the force angle and the friction angle of f_1. Note that although the direction of the contact force (or the force angle) varies from 5 to 20 degrees, the planned rolling motion keeps the friction angle within ± 5 degrees.

5.3 Discussions

Theoretical analysis, computer simulation, and experimental implementation are the three principal methodologies commonly utilized in robotics. In this paper, control of rolling contacts in multi-arm manipulation is investigated by employing all the three methodologies. In particular, the simulation and experiment results for the same manipulation task are reported. This provides a basis for comparison. In addition to verifying the control and planning algorithms developed from theoretical analysis, we are able evaluate the usefulness of computer simulations.

Comparing the figures depicting the simulation and experiment results, we have the following observations. There is a close match in the position trajectories between the simulation results (Figure 7) and the experiment results (Figure 11). Comparing Figures 8 and 12, on one hand, the simulation poorly predicts the behaviors of the physical system. On the other hand, the continuous lag displayed in Figure 8 is a clear indication that, when implementing the same control and planning algorithms on the physical system, the errors ϕ_1 and ϕ_2 are expected to be even larger, because of modeling parameter errors and unmodeled dynamics.

There are several reasons for the discrepancies between the simulation results and the experimental results. First the nonlinearity in the dynamics of the hardware (PUMA 250s) were not modeled. There is significant friction and backlash in the transmission and the noise in the contact force measurements is quite clear in Figure 13. While the backlash results in poor repeatability and accuracy this does not explain all the errors in the position trajectories in Figure 11. The errors due to backlash were estimated to much less than 1 mm and therefore are clearly much smaller than the 10 mm errors seen in the figure. It should be noted that the object position and orientation shown in the figure are not directly measured. They are estimated from the joint encoder readings *and* the measurements of the contact location from the tactile sensor. The sensor is very noisy and this leads to significant errors in the object position. Finally we speculate that the unmodeled structural dynamics have a significant effect on the system response. The structural
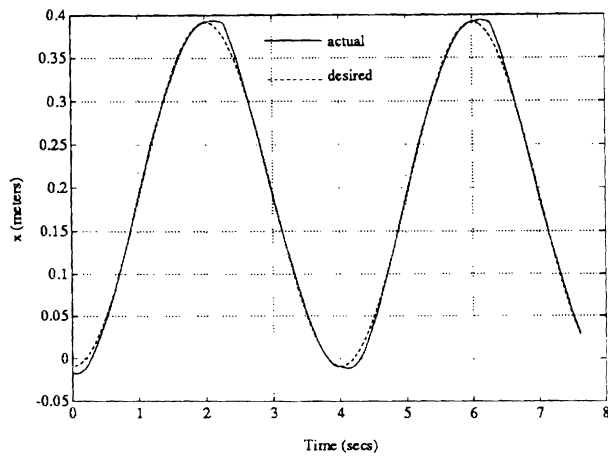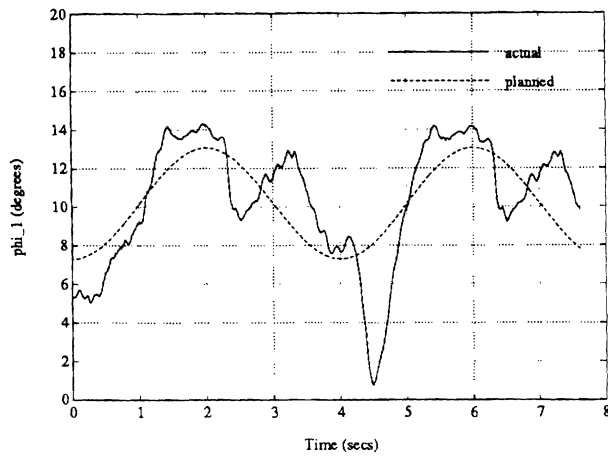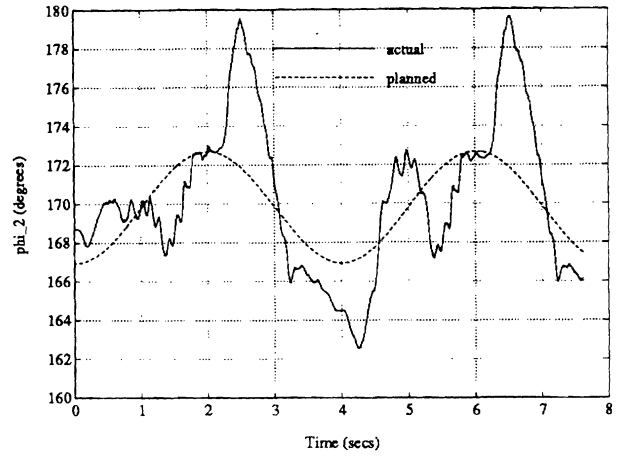
(a)
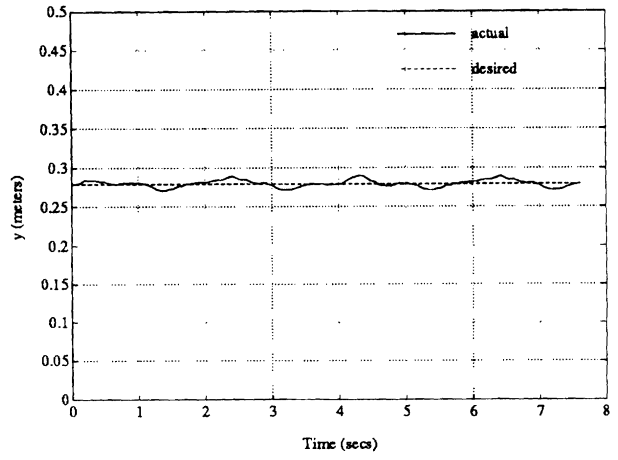
(b)
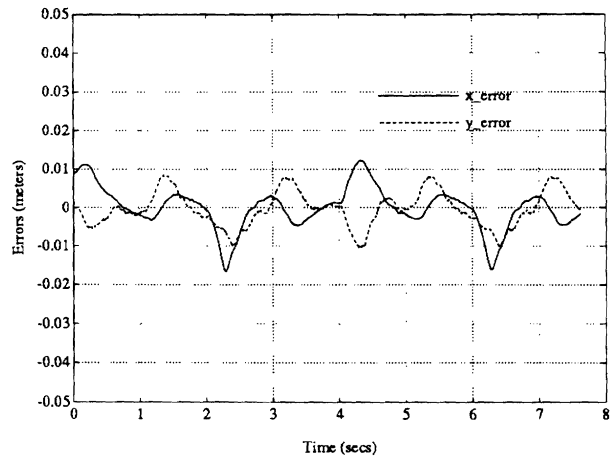
(c)

Figure 11: The position trajectories of the object from the experiment: (a) actual x_o, (b) actual y_o. (c) errors in x_o and y_o.
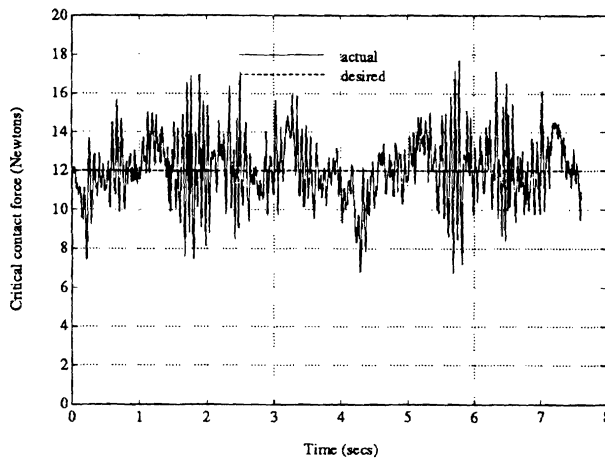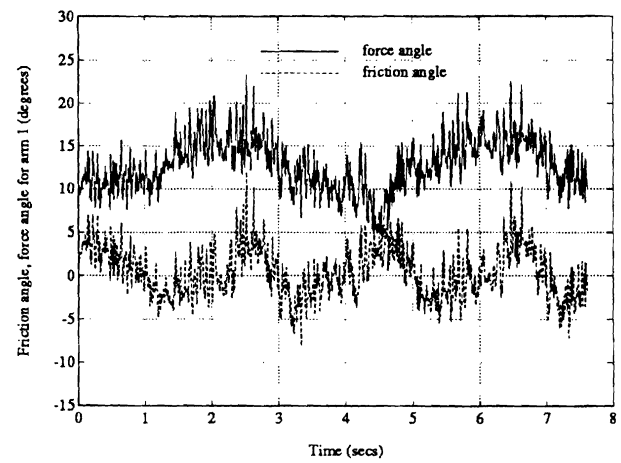
Figure 12: The planned and actual orientation trajectories of the two arms from the experiment: (a) ϕ_1 of arm 1, (b) ϕ_2 of arm 2.

Figure 13: The trajectories of the critical contact force f_{cc}, and the friction angles and force angle of f_1 from the experiment.

vibration modes coupled with the friction and backlash nonlinearities make the PUMA 250 a poor experimental test-bed. In spite of this the experimental results are according to predictions. The model-based control system is effective in controlling the contact forces and the trajectory and the friction angle is successfully decreased by the planner.

6 Concluding Remarks

We have presented the planning and control for the coordination of multiple arms in manipulation tasks involving rolling contacts. The planner determines optimal contact point locations on the effector and the object for a given task. The control algorithm, which is based on nonlinear feedback that decouples and linearizes the system, simultaneously controls the system trajectory (which includes the object trajectory as well as the trajectory of the contact points) and the constraint forces in order to maintain rolling contacts. We note that the force is controlled dynamically within the system as opposed to being statically compensated. A general mathematical formulation for the system dynamics is formulated. Our approach to control and planning are illustrated using two planar 3-R robot arms with a cylindrical object. Both simulation and experimental results are presented.

While much of the paper was limited to planar grasps with two point-contacts, we note that this is the first study of dual arm manipulation with grasps with rolling contacts that require the condition of force closure to be dynamically maintained by the controller. Further the adaptation of the grasp *via* rolling to external loads and the changing trajectory is presented here for the first time. Finally, the general framework presented in this paper is well-suited to pursuing multi-effector enveloping grasps.

An obvious extension to this work is the control and planning of three-dimensional grasps with rolling contacts. The theoretical basis for nonholonomic systems can be found in [1, 39, 36, 5] and some of our work in this direction is reported in [40]. The extension to more complicated objects is not very difficult. The key is to obtain analytical descriptions of the object surface in the neighborhood of each contact point. Extending this work to multiple contacts poses challenges, especially when more than one contacts occur on the same effector. A preliminary investigation of the dynamics of such systems is reported in [49].

Acknowledgment

References

[1] Anthony Bloch and N. H. McClamroch. Control of mechanical systems with classical non-holonomic constraints. In *Proceedings of 28th IEEE Conference on Decision and Control*, pages 201–205, Tampa, Florida, December 1989.

[2] C. Cai and B. Roth. On the spatial motion of rigid bodies with point contact. In *Proceedings of 1987 International Conference on Robotics and Automation*, pages 686–695, Raleigh, North Carolina, March 1987.

[3] L. Cai and A. A. Goldenberg. An approach to force and position control of robot manipulators. In *Proceedings of 1990 International Conference on Robotics and Automation*, pages 86–91, Cincinnati, OH, May 1990.

[4] A. Cole, J. Hauser, and S. Sastry. Kinematics and control of multifingered hands with rolling contact. In *Proceedings of 1988 International Conference on Robotics and Automation*, pages 228–233, Philadelphia, PA, April 1988.

[5] B. d'Andrea-Novel, B. Bastin, and G. Campion. Dynamic feedback linearization of nonholonomic wheeled mobile robots. In *Proceedings of 1992 International Conference on Robotics and Automation*, pages 2527–2532, Nice, France, May 1992.

[6] B. d'Andrea-Novel, G. Bastin, and G. Campion. Modelling and control of non holonomic wheeled mobile robots. In *Proceedings of 1991 International Conference on Robotics and Automation*, pages 1130–1135, Sacramento, CA, April 1991.

[7] C. Canudas de Wit and R. Roskam. Path following of a 2-DOF wheeled mobile robot under path and input torque constraints. In *Proceedings of 1991 International Conference on Robotics and Automation*, pages 1142–1147, Sacramento, CA, April 1991.

[8] J. Demmel and G. Lafferriere. Optimal three fingered grasps. In *Proceedings of the IEEE International Conference on Robotics and Automation*, Scottsdale, AZ, May 1989.

[9] B. R. Donald. *Error Detection and Recovery in Robotics*. Springer-Verlag, 1989.

[10] W. Holzmann and J.M. McCarthy. Computing the friction forces associated with a three fingered grasp. *IEEE Journal of Robotics and Automation*, RA-1(4), 1985.

[11] P. Hsu, Z. Li, and S. Sastry. On grasping and coordinated manipulation by a multifingered robot hand. In *Proceedings of 1988 International Conference on Robotics and Automation*, pages 384–389, Philadelphia, PA, April 1988.

[12] Yan-Ru Hu and A. A. Goldenberg. An adaptive approach to motion and force control of multiple coordinated robot arms. In *Proceedings of 1989 International Conference on Robotics and Automation*, pages 1091–1096, Scottsdale, Arizona, May 1989.

[13] A. Isidori. *Nonlinear Control Systems: An Introduction*. Springer-Verlag, Berlin, New York, 1985.

[14] J. Kerr and B. Roth. Analysis of multifingered hands. *Int. J. of Robotics Research*, 4(4), 1986.

[15] O. Khatib. A unified approach for motion and force control of robot manipulator: the operational space formulation. *Journal of Robotics and Automation*, RA-3(1):43–53, February 1987.

[16] C. Klein and S. Kittivatcharapong. Optimal force distribution for the legs of a walking machine. *IEEE Journal of Robotics and Automation*, 6(1):73–85, February 1990.

[17] A. J. Koivo and G. A. Bekey. Report of workshop on coordinated multiple robot manipulators: planning, control, and application. *IEEE Journal of Robotics and Automation*, 4(1):91–93, February 1988.

[18] V. Kumar. Wrench decompositon for multiple robotic systems. *IEEE Transactions on Robotics and Automation*, 1990. (under review). Also presented at the Workshop on Kinematics and Robotics, Lambrecht, W.Germany, June, 1990.

[19] V. Kumar and K. J. Waldron. Force distribution in closed kinematic chains. *IEEE Journal of Robotics and Automation*, 4(6), December 1988.

[20] V. Kumar and K. J. Waldron. Suboptimal algorithms for force distribution in multifingered grippers. *IEEE Journal of Robotics and Automation*, 5(4), August 1989.

[21] V. Kumar and K.J. Waldron. Force distribution in walking vehicles. *ASME Journal of Mechanical Design*, July 1990.

[22] K. Laroussi, H. Hemami, and R.E. Goddard. Coordination of two planar robots in lifting. *IEEE Transactions of Robotics and Automation*, 4(1), feb 1988.

[23] J.C. Latombe. *Robot motion planning*. Kluwer Academic Publishers, Boston, Massachussetts, 1991.

[24] Z. Li and S. Sastry. Task oriented optimal grasping by multifingered robot hands. *IEEE Transactions of Robotics and Automation*, 4(1), February 1988.

[25] Zexiang Li and John Canny. Motion of two rigid bodies with rolling constraint. *IEEE Transactions on Robotics and Automation*, 6(1):62–72, February 1990.

[26] T. Lozano-Perez, M. Mason, and R. Taylor. Automatic synthesis of fine motion strategies for robots. *International Journal of Robotics Research*, 3(1), 1984.

[27] J.Y.S. Luh and J.F. Zheng. Constraint relations between two coordinated industrial robots for motion control. *Int. J. of Robotics Research*, 6(3), 1987.

[28] David J. Montana. The kinematics of contact and grasp. *The International Journal of Robotics Research*, 7(3):17–32, June 1988.

[29] V. D. Nguyen. Constructing force-closure grasps. In *Proceedings of 1987 International Conference on Robotics and Automation*, Raleigh, N.C., April 1987.

[30] D.E. Orin and F.T. Cheng. General dynamic formulation of the force distribution equations. In *Advanced Robotics 1989, Proceedings of the Fourth International Conference on International Robotics*, pages 525–545, Columbus, Ohio, June 1989.

[31] Eric Paljug, Tom Sugar, Vijay Kumar, and Xiaoping Yun. Some important considerations in force control implementation. In *1992 IEEE International Conferfence on Robotics and Automation*, pages 1270–1275, Nice, France, May 1992.

[32] Eric Paljug and Xiaoping Yun. TRACS: two robotic arm coordination system. In *Video Proceedings of the IEEE International Conference on Robotics and Automation*, Sacramento, California, April 1991.

[33] Eric Paljug, Xiaoping Yun, and Vijay Kumar. Control of rolling contacts in multiple robotic manipulation. In *Proceedings of the International Conference on Advanced Robotics*, pages 591–596, Pisa, Italy, 1991.

[34] L. A. Pars. *A Treatise on Analytical Dynamics*. Wiley, New York, 1968.

[35] Mark E. Pittelkau. Adaptive load-sharing force control for two-arm manipulators. In *Proceedings of 1988 International Conference on Robotics and Automation*, pages 498–503, Philadelphia, PA, April 1988.

[36] S. K. Saha and J. Angeles. Dynamics of nonholonomic mechanical systems using a natural orthoganal complement. *Transactions of the ASME, Journal of Applied Mechanics*, 58:238–243. March 1991.

[37] J.K. Salisbury, W. Townsend, B. Eberman, and D. DiPietro. Preliminary design of a whole arm manipulation system. In *1988 International Conference on Robotics and Automation*, pages 254–260, Philadelphia, PA, April 1988.

[38] K. Salisbury and B. Roth. Kinematics and force analysis of articulate mechanical hands. *ASME Journal of Mechanisms, Transmissions and Automation in Design*, 105:35–41, March 1983.

[39] C. Samson and K. Ait-Abderrahim. Feedback control of a nonholonomic wheeled cart in cartesian space. In *Proceedings of 1991 International Conference on Robotics and Automation*, pages 1136–1141. Sacramento, CA, April 1991.

[40] Nilanjan Sarkar, Xiaoping Yun, and Vijay Kumar. *Control of Mechanical Systems with Rolling Constraints: Application to Dynamic Control of Mobile Robots*. Technical Report MS-CIS-92-44, GRASP LAB 320. Department of Computer and Information Science, University of Pennsylvania, Philadelphia, PA 19104, 1992.

[41] S.A. Schneider and R.H. Cannon. Object impedance control for cooperative manipulation. In *Proceedings of the IEEE International Conference on Robotics and Automation*, Scottsdale, AZ, May 1989.

[42] M. Spong and M. Vidyasagar. *Robot Dynamics and Control*. John Wiley and Sons, New York, 1989.

[43] Il Hong Suh and Kang G. Shin. Coordination of dual robot arms using kinematic redundancy. In *Proceedings of 1988 International Conference on Robotics and Automation*, pages 504–509, Philadelphia, PA. April 1988.

[44] T. J. Tarn, A. K. Bejczy, and X. Yun. Design of dynamic control of two cooperating robot arms: closed chain formulation. In *Proceedings of 1987 International Conference on Robotics and Automation*, pages 7–13, Raleigh, North Carolina, March 1987.

[45] N. Ulrich and V. Kumar. Grasping using fingers with coupled joints. In *Proceedings of the 1988 ASME Mechanisms Conference*, Orlando, Florida, September 1988.

[46] M. A. Unseren and A. J. Koivo. Reduced order model and decoupled control architecture for two manipulators holding an object. In *Proceedings of 1989 International Conference on Robotics and Automation*, pages 1240–1245, Scottsdale, Arizona, May 1989.

[47] I.D. Walker, R.A. Freeman, and S.I. Marcus. Internal object loading for multiple cooperating robot manipulators. In *Proceedings of the IEEE International Conference on Robotics and Automation*, Scottsdale, AZ, May 1989.

[48] M.W. Walker, D. Kim, and J. Dionise. Adaptive coordinated motion control of two manipulator arms. In *Proceedings of the IEEE International Conference on Robotics and Automation*, Scottsdale, AZ, May 1989.

[49] Y. Wang, V. Kumar, and J. Abel. Dynamics of rigid bodies undergoing multiple frictional contacts. In *IEEE International Conference on Robotics and Automation*, May 1992.

[50] J. Wen and K. Kreutz. Motion and force control for multiple cooperative manipulators. In *Proceedings of the IEEE International Conference on Robotics and Automation*, Scottsdale, AZ, May 1989.

[51] T. Yoshikawa and K. Nagai. Evaluation and determination of the grasping forces in a multi-fingered grasp. In *Proceedings of 1988 International Conference on Robotics and Automation*, pages 245–248, Philadelphia, PA, April 1988.

[52] Xiaoping Yun, Vijay Kumar, Nilanjan Sarkar, and Eric Paljug. Control of multiple arms with rolling constraints. In *1992 IEEE International Conferfence on Robotics and Automation*, pages 2193–2198, Nice, France, May 1992.

[53] Xiaoping Yun and Vijay R. Kumar. An approach to simultaneous control of trajectory and interaction forces in dual arm configurations. *IEEE Transactions on Robotics and Automation*, 7(5):618–625, October 1991.

[54] Y. Zheng and J.Y.S. Luh. Optimal load distribution for two industrial robots handling a single object. In *IEEE International Conference on Robotics and Automation*, Philadelphia, PA, April 1988.

A Derivation of the Error Bound in the Critical Contact Force

Taking the projection of the translational object motion equation (top two rows of Equation (6)) upon e_{12} yields

$$(m_o \ddot{r}_t - w_f) \cdot e_{12} = (f_1 + f_2) \cdot e_{12} \tag{36}$$

where $r_t = [x_O \ y_O]$ and w_f is the first two elements of W. This expression can be combined with Equation (20) such that the $f_2 \cdot e_{12}$ term is eliminated. The resulting expression solved for $f_1 \cdot e_{12}$ is given as:

$$f_1 \cdot e_{12} = f_{cc} + \frac{1}{2}|(m_o \ddot{r}_t - w_f) \cdot e_{12}| + \frac{1}{2}(m_o \ddot{r}_t - w_f) \cdot e_{12} \tag{37}$$

This expression also serves as a planner for the desired $f_1 \cdot e_{12}$ which is written as:

$$f_1^d \cdot e_{12} = f_{cc}^d + \frac{1}{2}|(m_o^d \ddot{r}_t^d - w_f^d) \cdot e_{12}| + \frac{1}{2}(m_o^d \ddot{r}_t^d - w_f^d) \cdot e_{12} \tag{38}$$

The error terms are defined as:

$$e_{cc} = f_{cc}^d - f_{cc} \tag{39}$$

$$e_1 = (f_1^d - f_1) \cdot e_{12} \tag{40}$$

$$e_r = \ddot{r}_t^d - \ddot{r}_t \tag{41}$$

$$e_w = (w_f^d - w_f) \cdot e_{12} \tag{42}$$

and the modeled mass as $m_o^d = m_o + \Delta m_o$ where Δm_o represents any model discrepancies. The expression for the error in the critical contact force is then written as:

$$\begin{aligned}
e_{cc} = & f_1^d \cdot e_{12} - \frac{1}{2}|(m_o^d \ddot{r}_t^d - w_f^d) \cdot e_{12}| - \frac{1}{2}(m_o^d \ddot{r}_t^d - w_f^d) \cdot e_{12} \\
& - \left[f_1 \cdot e_{12} - \frac{1}{2}|(m_o \ddot{r}_t - w_f) \cdot e_{12}| - \frac{1}{2}(m_o \ddot{r}_t - w_f) \cdot e_{12} \right]
\end{aligned} \tag{43}$$

By expanding m_o^d and gathering common terms, the above equation can be written as:

$$\begin{aligned}
e_{cc} = & f_1^d \cdot e_{12} - f_1 \cdot e_{12} - \frac{1}{2} m_o \ddot{r}_t^d \cdot e_{12} + \frac{1}{2} m_o \ddot{r}_t \cdot e_{12} \\
& - \frac{1}{2} w_f^d \cdot e_{12} - \frac{1}{2} w_f \cdot e_{12} - \frac{1}{2}|m_o \ddot{r}_t^d \cdot e_{12} - w_f^d \cdot e_{12} + \Delta m_o \ddot{r}_t^d \cdot e_{12}| \\
& + \frac{1}{2}|m_o \ddot{r}_t \cdot e_{12} - w_f \cdot e_{12}| - \frac{1}{2} \Delta m_o \ddot{r}_t^d \cdot e_{12}
\end{aligned} \tag{44}$$

By taking the norm of both sides, a bound is found for the error in the critical contact force:

$$\|e_{cc}\| \leq \|e_1\| + \|m_o\| \, \|e_r\| \, \|e_{12}\| + \|e_w\| + \|\Delta m_o\| \, \|\ddot{r}_t^d\| \, \|e_{12}\| \tag{45}$$

Thus, the error in the critical contact force is bounded by the sum of the object trajectory error, the error in f_1 along e_{12}, the disturbance error, and the object modeling error. Note that Equation (38) which includes a non-differentiable function is used in the planner. However, this function does not appear in the output equation or state equation of the system.

B Robot Parameters

This appendix presents the kinematic and dynamic parameters for two PUMA 250s which are used to implement the nonlinear feedback control law. Joint 2, 3, and 5 are made parallel as shown in Figure 14 while joint 1, 4, and 6 are locked. Thus, the PUMA 250 (with the three joints locked) form the three planar links of the 3-R manipulator in Figure 2, with the corresponding axis marked 3R AXIS 1, 2, or 3 in Figure 14. For convenience, the three links will be numbered 1, 2, and 3. In the figure, l_1, l_2, and l_3 denotes the corresponding link lengths.

All the parameters are listed in Table 1. Although the two manipulators are identical, robot 1 has a force/torque sensor installed at the wrist while robot 2 does not. Thus two sets of parameter values are listed if they are different. Before the joint torques computed from the nonlinear feedback are sent to the Digital-to-Analog Converter (DAC), they are multiplied by the torque constants. The friction constants are the DAC values corresponding to the Coulomb friction at the joints. All the parameters listed in Table 1 are experimentally measured.

Parameters	Link Number i	Values Robot 1 / Robot 2	Units
Link Length (l_i)	1	203	mm
	2	203	mm
	3	93 / 63	mm
Link Mass	1	2.4	Kg
	2	1.1	Kg
	3	0.54 / 0.2	Kg
Center of Mass	1	30	mm
	2	60	mm
	3	54 / 12	mm
Link Inertia	1	0.145	Kg-m^2
	2	0.052	Kg-m^2
	3	0.00727 / 0.00527	Kg-m^2
Torque Constant	1	103 / 138	DAC/N-m
	2	140 / 210	DAC/N-m
	3	-1633 / -980	DAC/N-m
Friction Constant	1	-116 / -116	DAC
	2	-95 / -100	DAC
	3	-160 / -105	DAC
Tactile Sensor Gain		$5.094 \cdot 10^{-5}$ / $5.145 \cdot 10^{-5}$	mm/DAC
Tactile Sensor Offset		-0.15317 / -0.15558	mm

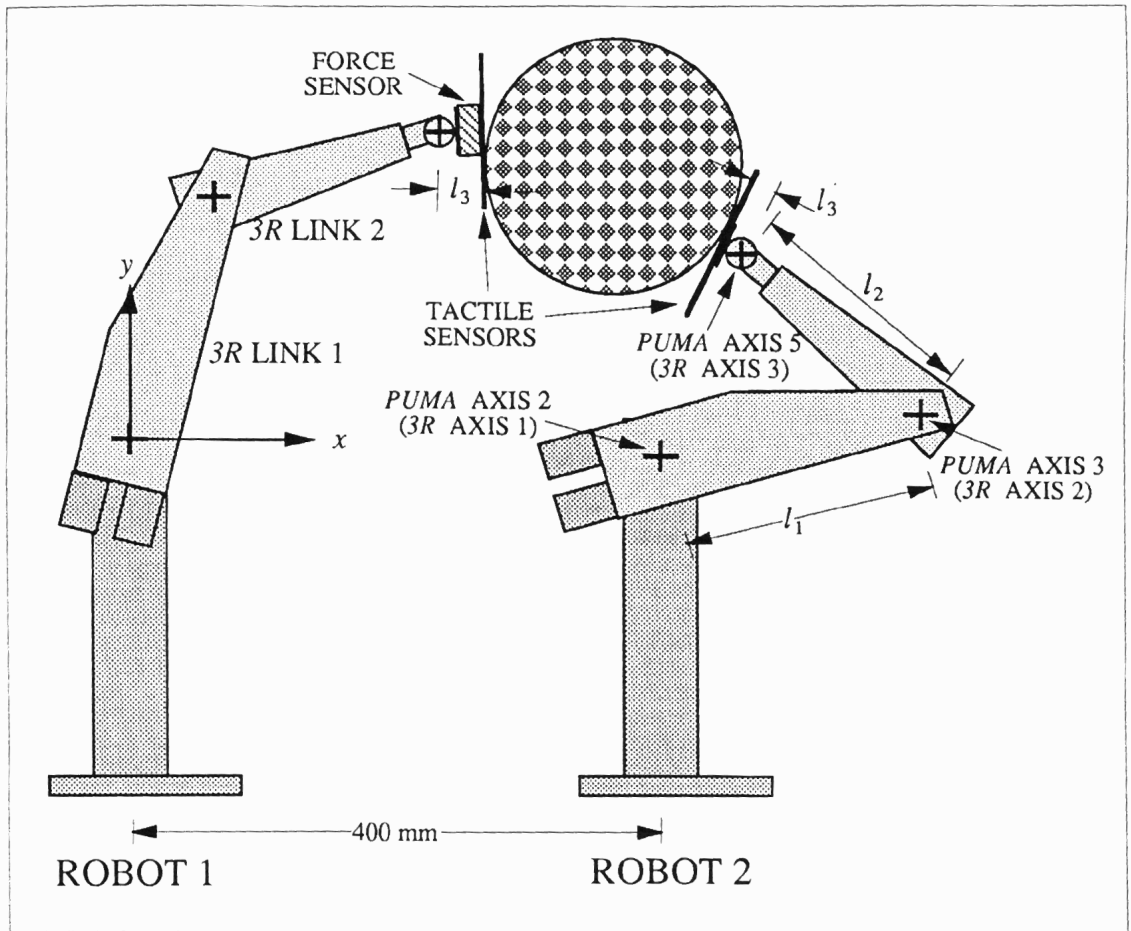Table 1: Parameters for the three links of the PUMA 250s used in the experiment.

Figure 14: Sketch of experimental set-up.